A Reduced-Complexity Description of Arm Endpoint Stiffness with Applications to Teleimpedance Control

Arash Ajoudani, Cheng Fang, Nikos G. Tsagarakis, and Antonio Bicchi

***Abstract*— Effective and stable execution of a remote manipulation task in an uncertain environment requires that the task force and position trajectories of the slave robot be appropriately commanded. To achieve this goal, in teleimpedance control, a reference command which consists of the stiffness and position profiles of the master is computed and realized by the compliant slave robot in real-time. This highlights the need for a suitable and computationally efficient tracking of the human limb stiffness profile in real-time. In this direction, based on the observations in human neuromotor control which give evidence on the predominant use of the arm configuration in directional adjustments of the endpoint stiffness profile, and the role of muscular co-activations which contribute to a coordinated regulation of the task stiffness in all directions, we propose a novel and computationally efficient model of the arm endpoint stiffness behaviour. Real-time tracking of the human arm kinematics is achieved using an arm triangle monitored by three markers placed at the shoulder, elbow and wrist level. In addition, a co-contraction index is defined using muscular activities of a dominant antagonistic muscle pair. Calibration and identification of the model parameters are carried out experimentally, using perturbation-based arm endpoint stiffness measurements in different arm configurations and co-contraction levels of the chosen muscles. Results of this study suggest that the proposed model enables the master to naturally execute a remote task by modulating the direction of the major axes of the endpoint stiffness and its volume using arm configuration and the co-activation of the involved muscles, respectively.**

I. Introduction

The need to manipulate objects and tools in unstructured or hostile environments has lead to the development of several Master-Slave teleoperation interfaces: from the most basic, unilateral position-based, to bilateral force-reflecting systems. Notwithstanding the widespread use of such frameworks, they are known to lack substantial requirements to render an appropriate interaction performance (e.g. soft interactions in unilateral and stability in the latter [1], [2]). In an attempt to overcome the limitations of conventional teleoperation interfaces, the concept of teleimpedance control has been recently introduced [3], [4], with several interaction scenarios in support of the efficacy of this control concept [3], [5], [6].

Arash Ajoudani, Cheng Fang, Nikos G. Tsagarakis and Antonio Bicchi are with the Dept. of Advanced Robotics, Istituto Italiano di Tecnologia, Via Morego 30, 16163, Genova, Italy. Arash Ajoudani and Antonio Bicchi are also with Interdepartmental Research Center "E. Piaggio", Faculty of Engineering, University of Pisa, Italy. e-mails: arash.ajoudani@iit.it, cheng.fang@iit.it, nikos.tsagarakis@iit.it and bicchi@centropiaggio.unipi.it.

This work is supported in part by the European Research Council under the Advanced Grant SoftHands "A Theory of Soft Synergies for a New Generation of Artificial Hands" no. ERC-291166, and by the EU FP7 project (601165), "WEARable HAPtics for Humans and Robots (WEARHAP)".

To establish such an interface, an aggregate reference command that includes the desired motion trajectories and impedance profiles of the operator is realized by a compliant slave robot in real-time. Unlike the results and continuous improvements in implementation of various control frameworks that enable a robust and effective interaction performance in active, passive or hybrid compliant robots, a bigger issue, i.e. a suitable, real-time and computationally efficient modelling of the master's stiffness profile remains to be done.

It is well known that humans modulate their limb endpoint visco-elastic properties in different ways. One approach to achieve this is by co-contracting muscle groups acting on the limb [7]. Alternatively, it is performed through the adaptation in the sensitivity of reflex feedback [8] or selective control of the limb configuration [9]. Traditionally, the combined effect of the above stiffness modulation mechanisms at the arm endpoint is explored by applying position (force) perturbations to the hand, and probing the restoring force (displacement response) profile [10], [11]. This is usually followed by an off-line post-processing phase to estimate the impedance parameters. Application of such methods in estimation of dynamic impedance profiles in multi-joint arm movements has been extensively investigated [12].

Despite the popularity of the perturbation based approaches, their real-time applications result in an inconvenient and often impossible operation due to the interference of the external disturbance with the hand trajectories. As a consequence, other avenues of research seek for a more suitable Human Machine Interface (HMI) that is particularly beneficial for real-time applications [3], [13], [14]. In this direction, due to the existence of high correlations between the muscle activations, muscular force and joint torque profiles, a large portion of related literature utilize electromyography (EMG) signals to account for real-time tracking of the arm joint/endpoint stiffness profile. While in a fixed arm configuration, such a modelling turns out to be straightforward due to the linear association between the EMG and arm endpoint stiffness profiles [15], the whole arm workspace stiffness estimation appears to require a complex modelling of the musculo-skeletal system [13], [16]. This, however, contrasts with several studies on human motor behaviour which suggest that the central nervous system (CNS) solves for this complexity and redundancy in an elegant, effective and coordinated manner [17], [18].

Observations in human neuromotor control of the arm endpoint stiffness suggest that due to i) the major contribution of the limb geometry to efficient modifications in the orientation

of the endpoint stiffness ellipsoid, ii) ergonomic efficiency of postural adjustments in comparison to co-contractions, and iii) the existence of cross–joint muscles in limbs, humans tend to maximize the use of limb postures to realize a desired endpoint stiffness direction [19]. Concurringly, co-contractions appear to mostly contribute to modifications in size, rather than orientation of the stiffness ellipsoid [3], [19]. A reason for that is deemed to be the involvement of the arm muscles in a synergistic fashion [18], [20]–[22], which contribute to coordinated variations in the diagonal (joint stiffness) and off-diagonal (due to the existence of cross-joint muscles) components of the joint stiffness matrix.

On these bases, we explore the role of arm geometry and muscular contraction in modifications in directionality and size of the arm endpoint stiffness ellipsoid, respectively. To do so, we investigate the configuration-dependent properties of the joint and Cartesian stiffness profiles in humans and illustrate that directional variations of the endpoint stiffness ellipsoid are predominantly influenced by the arm Jacobian than the pose-varying component of the joint stiffness. Consequently, with the purpose of minimizing the number of tracking points in human arm to account for the arm geometry, an arm triangle model is introduced and used for the estimation of joint angles and the arm Jacobian. On the other hand, a co-contraction index is defined and experimentally identified that appoint to the size-adjusting component of the arm endpoint stiffness.

Having the two models identified, the endpoint stiffness of the human arm is estimated by tracking the arm Jacobian and the co-contraction index in real time. This enables the master to modify the direction of the endpoint stiffness ellipsoid by changing the arm posture, while being capable of adjusting its volume by increasing the co-activation of the dominant arm muscles. As a result, teleoperated tasks which require significant modulation of the endpoint stiffness and force can be executed effectively and naturally.

II. Dimensionality Reduction in Endpoint Stiffness Representation

It is well-known that in a steady muscular contraction, the arm geometry affects both the joint and endpoint stiffness behaviour. While the configuration-dependent nature of the joint stiffness is mainly caused by the variations in passive joint properties such as moment arms, muscle and tendon lengths, the calculation of the Cartesian stiffness on the other hand, requires an additional transformation which is provided by the arm Jacobian.

To investigate the geometric dependency of the joint and Cartesian stiffness profiles, we address the transformation for the joint and Cartesian stiffness of the human arm for two nearby equilibriums $[q_0, K_J(p,q_0), K_c(p,q_0)]$ and $[q_0+\delta q, K_J(p,q_0+\delta q), K_c(p,q_0+\delta q)]$ (see [23], [24] for details)

$$\begin{aligned} &K_c(p,q_0+\delta q) = \\ &J^{+T}(q_0+\delta q)[K_J(p,q_0+\delta q) - G_J(q_0+\delta q)]J^{+}(q_0+\delta q), \end{aligned} \tag{1}$$

Here, $J \in \mathbb{R}^{6\times 7}$, $K_c \in \mathbb{R}^{6\times 6}$, $K_J \in \mathbb{R}^7$, and $q \in \mathbb{R}^7$ denote the arm Jacobian, Cartesian stiffness, joint stiffness and the joint angle vector, respectively. p is a co-contraction index which is considered steady in both configurations. q_0 and δq denote the initial and infinitesimal increment of the joint angle vector, respectively. $G_J(q)$ is defined by

$$G_J(q) = \frac{\partial J^T(q) f_0}{\partial q} + \frac{\partial \tau_g(q)}{\partial q}, \tag{2}$$

which captures the effect of external load f_0 and gravity $\tau_g(q)$ on Cartesian stiffness. A first order Taylor expansion of the Cartesian stiffness gives

$$K_c(p,q_0+\delta q) = K_c(p,q_0) + \left.\frac{\partial K_c(p,q)}{\partial q}\right|_{q=q_0} \delta q. \tag{3}$$

By computing the last term above, we obtain

$$\begin{aligned} &\left.\tfrac{\partial K_c(p,q)}{\partial q}\right|_{q_0} \delta q = \\ &\left.\tfrac{\partial J^{+T}(q)}{\partial q}\right|_{q_0} \delta q[K_J(p,q_0) - G_J(q_0)]J^{+}(q_0) + \\ &J^{+T}(q_0)[\left.\tfrac{\partial K_J(p,q)}{\partial q}\right|_{q_0} \delta q + \left.\tfrac{\partial G_J(q)}{\partial q}\right|_{q_0} \delta q]J^{+}(q_0) + \\ &J^{+T}(q_0)[K_J(p,q_0) - G_J(q_0)] \left.\tfrac{\partial J^{+}(q)}{\partial q}\right|_{q_0} \delta q, \end{aligned} \tag{4}$$

which explains that the pose-varying component of the joint stiffness matrix in Cartesian coordinates is reflected by the only relation

$$J^{+T}(q_0)[\left.\frac{\partial K_J(p,q)}{\partial q}\right|_{q_0} \delta q]J^{+}(q_0).$$

As observed in the above equations, the arm Jacobian has a quadratic effect in Cartesian stiffness behaviour. On the other hand, it has been illustrated that far from the arm joint limits, the muscle length and moment arm variations are fairly smooth and bounded [25], [26]. For instance, in the full range of angular displacements, the length of wrist and elbow muscles can change by 8.5% and 55%, respectively. However, in a proximity of the middle ranges of the arm joints (which the experiments will be conducted), this range is shifted towards smaller values [25]. These remarks imply that in a certain volume of the human arm workspace, the effect of arm geometry in directional variations of the principal axes of the Cartesian stiffness ellipsoid though Jacobian is more effective than the role of configuration-dependent joint stiffness term. Thus, in our model, we include the effect of arm Jacobian in directional variations of the major axes of the arm endpoint stiffness ellipsoid, and neglect the configuration-dependent effect of the joint stiffness matrix. This task-related decision is made based on the chosen trade off between the accuracy and modelling complexity.

Furthermore, solid evidence on the coordinated stiffening of the arm joints [3], [18], [20] which contributes to the modifications in the volume of the endpoint stiffness ellipsoid suggests that the active joint stiffness regulations can be modelled as $K_J = a_{cc}(p)\,\overline{K_J}$, with $\overline{K_J}$ corresponding to the joint stiffness matrix at minimum muscle activity, and $a_{cc}(p)$ a size-adjusting co-contraction index. Thus,

$$K_c(p,q) = J^{+T}(q)[a_{cc}(p)\,\overline{K_J} - G_J(q)]J^{+}(q). \tag{5}$$

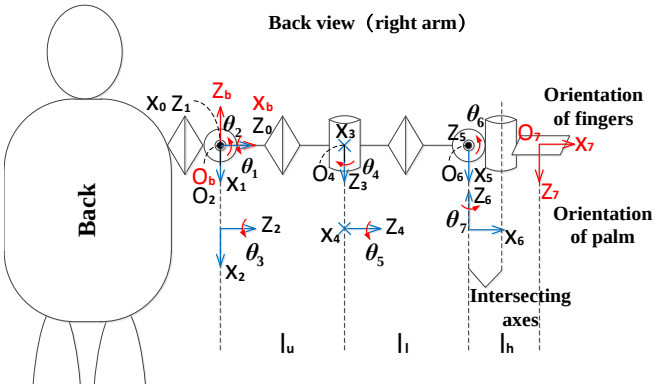

Fig. 1: Human arm kinematic model.

One of the objectives of this paper is to investigate the feasibility of the above model and illustrate that a fairly acceptable and real-time tracking of the human arm endpoint stiffness in 3D can be achieved using $\overline{K_J}$ (which will be experimentally identified), tracking of the arm configuration and the co-contraction index.

III. Human Arm Jacobian Tracking

As mentioned earlier, human limb kinematics play a dominant role in geometric regulations of the endpoint impedance and force ellipsoids [23]. As a result, so called "natural" postures emerge while humans execute tasks which require significant stiffness or force modulations. Therefore, to analyse the effect of arm configuration in regulations of K_c in (5), a model of the human arm Jacobian must be implemented.

One way to achieve this is to measure and track the arm joint angles in real-time. This is usually performed by attaching several optical tracking markers or position sensors to the human arm which brings discomfort and complexity. To avoid that, using our previous results in modelling and identification of the human arm kinematics in a rather simple but accurate way, a human arm triangle model is introduced and used for the calculation of $J(q)$ in real-time [27].

First, we establish a typical kinematic model for the human arm [28], as shown in Fig. 1. The corresponding DH parameters are presented in Table I. The values in the parentheses denote the offset angles of θ_i in a configuration which is depicted in Fig. 1. The link frames are established in a post-position manner. For convenience, the directions of the z_b, x_b and y_b axes of the base frame $\{b\}$ are considered upwards, horizontal right and horizontal forward, respectively. The origin of the frame $\{b\}$ is placed at the centre of the shoulder. The z_7 axis of the last frame $\{7\}$ coincides with the unit normal vector of the plane of palm, x_7 points in the direction of fingers, and y_7 points in the inverse direction of thumb. The origin of this frame is set to be the centre of the palm. In addition, l_u and l_l denote the lengths of the upper arm and the lower arm, respectively. l_h represents the length measured from the centre of the wrist to the centre of the palm.

Consequently, a human arm triangle model (see Fig. 2) is defined and used for the estimation of the joint angles,

TABLE I: DH Parameters of Human Arm Kinematic Model

$i(^{i-1}T_i)$	θ_i	d_i	a_i	α_i
0	-90°	0	0	-90°
1	$\theta_1(90^\circ)$	0	0	90°
2	$\theta_2(0^\circ)$	0	0	-90°
3	$\theta_3(90^\circ)$	l_u	0	90°
4	$\theta_4(0^\circ)$	0	0	-90°
5	$\theta_5(-90^\circ)$	l_l	0	90°
6	$\theta_6(90^\circ)$	0	0	-90°
7	$\theta_7(0^\circ)$	0	l_h	180°

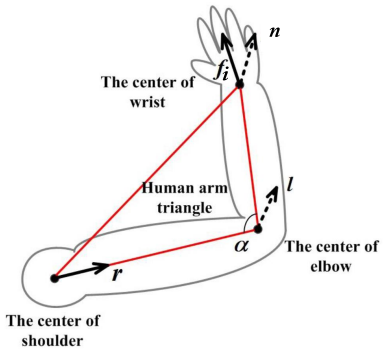

Fig. 2: Human arm triangle model.

and the Jacobian matrix. The human arm triangle model is expressed by five parameters:

r: unit direction vector of the upper arm.
l: unit normal vector of the plane of the human arm triangle. The direction of l is determined by the right-hand rule, and the right-hand screw direction is the direction of elbow extension.
α: the angle between the upper arm and lower arm.
fi: unit direction vector of the fingers.
n: unit normal vector of the plane of the palm. Its direction points outward from the centre of the palm.

It has been demonstrated that the human arm triangle space spanned by these five parameters has a one-to-one mapping relationship with the joint space spanned by the seven joint variables (see [27], [29] for details). Therefore, using this model and assuming that the shoulder base frame data is known, only wrist posture and elbow position measurements are necessary to complete the model.

Furthermore, using the weight and centre of mass of the segments of an average human arm [30], in this study, a rough estimate of the human arm gravitational torque is implemented using

$$\tau_g(q) = \sum_{i=1}^{n_J} J_{com_i}^T(q) g m_i, \tag{6}$$

with J_{com_i}, m_i, n_J and g being the centre of mass Jacobian and the mass of the ith limb, number of joints, and vector of gravitational accelerations, respectively. For more accu-

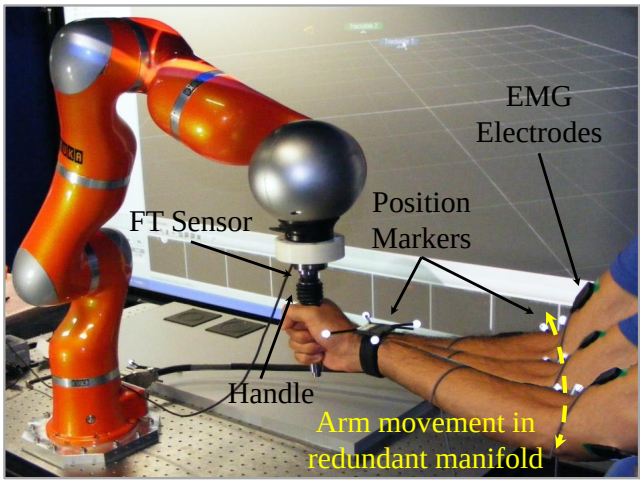

Fig. 3: Stiffness measurement experimental setup. KUKA lightweight robot was programmed to apply stochastic perturbations to the human hand. Experiments were carried out in different arm configurations with a fixed position/orientation of the wrist and shoulder. Arm joints were allowed to vary within the redundant manifold of the corresponding shoulder and wrist position. One subject participated in the experiments.

rate modelling of the arm gravitational torques in different configurations, alternative platforms such as OpenSim [31] can be utilized.

IV. Human Arm Endpoint Stiffness Estimation

This section describes the procedure to identify the minimum muscular contraction (minimum activity) joint stiffness matrix $\overline{K_J}$, and the co-contraction index $a_{cc}(p)$. As a result, a model of K_J is realized which contributes to the adjustments in size of the endpoint stiffness ellipsoid (K_c). In this direction, based on the observations in support of the coordinated activation of arm muscles in stiffness regulation tasks [7], [18], and the presence of high correlation between the active joint stiffness profiles and muscular activations which can be estimated using electromyography signals (EMGs), we acquire and process surface EMGs from a pair of antagonistic muscles in the forearm.

To identify $\overline{K_J}$ and $a_{cc}(p)$, assuming that $J(q)$ and $G_J(q)$ are calculated and known[1], K_c in (5) must be identified in different configurations[2] and co-contraction levels of the human arm. While the minimum-activity trials will be selected for the identification of $\overline{K_J}$, others will be utilized for the modelling and identification of the co-contraction index.

Following standard techniques in identification of human arm endpoint stiffness in 3D [11], stochastic perturbations were applied to the human wrist and restoring forces were recorded using a 6-axis force-torque sensor (ATI Inc.), which was placed between the robot and the handle (see Fig. 3). KUKA lightweight robot IV was programmed in position control mode using Fast Research Interface [32], aiming at applying perturbation profiles to the arm endpoint through a handle.

Experiments were carried out in eight different positions of the wrist w.r.t the shoulder frame. These configurations were chosen anterior to the coronal plane of the body, within a reasonable workspace of the human arm while avoiding singular configurations and joint limits. In each set, arm joints were allowed to vary within the redundant manifold of the corresponding shoulder-wrist configuration to realize three distinct elevation angles of the elbow joint (see Fig. 3), resulting in 24 arm configurations in total. At each configuration, the subject was asked to modulate and keep the co-activation of the arm muscles in three different levels: minimum-activity (0% $\|P_{max}\|$), Mid (30% $\|P_{max}\|$) and High (60% $\|P_{max}\|$), generating 72 trials in total, some of which repeated for testing purposes. $\|P_{max}\|$ is the maximum value of the co-contraction indicator and is calculated by the norm[3] of the processed (acquired, filtered and normalized at 700 Hz; see [3] for details) EMG signals from two dominant, antagonistic upper arm muscles; namely Biceps (P_B) and Triceps (P_T) Brachii, hence

$$\|P\| = \|[P_B \;\; P_T]\|.$$

Throughout the experiments, $\|P\|$ was illustrated to the subject to keep the co-contraction levels as steady as possible. Meanwhile, body-markers were attached to the human wrist, elbow and shoulder for synchronized and precise tracking of the i) human hand trajectories under perturbations and ii) human arm Jacobian, using Optitrack motion tracking system at 200 Hz. Acquisition, processing, control, and synchronization algorithms were all implemented in C++.

Consequent to the acquisition and pre-processing of the position and restoring force trajectories of the human arm endpoint, multiple–input multiple–output (MIMO) dynamics of the endpoint impedance was decomposed into the linear subsystems associating each input to each output [3]. Based on this assumption, and indicating with $F_x(f)$, $F_y(f)$ and $F_z(f)$ the Fourier transforms of the endpoint force along the axes of the Cartesian reference frame, with $x(f)$, $y(f)$ and $z(f)$ the transforms of the human endpoint displacements, the dynamic relation between the displacements and force variations can be described by

$$\begin{bmatrix} F_x(f) \\ F_y(f) \\ F_z(f) \end{bmatrix} = \begin{bmatrix} G_{xx}(f) & G_{xy}(f) & G_{xz}(f) \\ G_{yx}(f) & G_{yy}(f) & G_{yz}(f) \\ G_{zx}(f) & G_{zy}(f) & G_{zz}(f) \end{bmatrix} \begin{bmatrix} x(f) \\ y(f) \\ z(f) \end{bmatrix}. \qquad (7)$$

A non-parametric algorithm was adopted to identify the empirical transfer function of each of the SISO subsystems described above in frequency domain (MATLAB, The MathWorks Inc.). The smoothed spectral estimates of input and outputs (using windowing techniques) were fed to this algorithm in order to identify each SISO transfer function.

[1]We assume that no endpoint forces are generated or applied to the human arm. Thus $f_0 = 0$ in (2).

[2]To strengthen our assumption on the negligence of the pose-varying component of the joint stiffness (through moment arms and muscle-tendon lengths), the experiments will be carried out in a reasonable workspace of the human arm, avoiding extreme extension or flexion of the arm joints.

[3]In this paper, the operator ($\|.\|$) refers to the Frobenius norm.

Consequently, we adopted a parametric, second order, linear model of each impedance transfer function of the type

$$G_{ij}(s) = I_{cij}s^2 + B_{cij}s + K_{cij}, \quad s = 2\pi f\sqrt{-1} \tag{8}$$

where I_c, B_c and K_c denote the endpoint inertia, viscosity and stiffness matrices, respectively. The parameters of the second order linear model were identified based on least squares algorithm in frequency range from 0 to 10Hz.

In a post-processing stage, identified Cartesian stiffness matrices from the minimum activity trails were used to compute $\overline{K_J}$ by minimizing

$$\|\overline{K_J} - J^T(q)K_cJ(q) - \frac{\partial \tau_g(q)}{\partial q}\|. \tag{9}$$

On the other hand, to identify $a_{cc}(p)$ from Mid and High muscular activity trials, a modified hyperbolic tangent function of P_B and P_T is used. This choice is due to the simplicity, flexibility and capability of this model in the generation of various (saturated) output profiles [6], [33]. Hence,

$$a_{cc}(p) = 1 + \frac{c_1[1 - e^{-c_2(P_B+P_T)}]}{[1 + e^{-c_2(P_B+P_T)}]}, \tag{10}$$

with c_1 and c_2 being constant coefficients that can be identified by minimizing

$$\|a_{cc}(p)\,\overline{K_J} - J^T(q)K_cJ(q) - \frac{\partial \tau_g(q)}{\partial q}\|. \tag{11}$$

V. Results

In this section, we evaluate the results of the identification of the proposed model in a teleimpedance control setup. We demonstrate that even though the calibrated model is subject to uncertainty due to the i) use of minimum number of muscles to account for the co-contraction index, and ii) negligence of the pose-varying effect of K_J, it still provides the master with an intuitive and efficient capability to realize a desired task stiffness profile using his/her arm pose and co-activation of the involved muscles.

A. Identification Results

Experimental identification of the endpoint impedance matrices was performed by applying position perturbations and acquiring the force response within 10 Hz frequency range. In all trials, multiple and partial coherence values of the force-position data (see Fig. 4), positive definiteness and symmetric[4] measures of the estimated impedance matrices [3], [11] were the proving factors for the feasibility of the acquired results. Those trails which did not satisfy the above conditions were discarded and repeated. Consequently, identified stiffness matrices and the corresponding human arm Jacobian were used for the identification of $\overline{K_J}$ and $a_{cc}(p)$.

[4]By calculating $\frac{K_c - K_c^T}{K_c + K_c^T}$ which resulted in an average value of 0.12 overall trials.

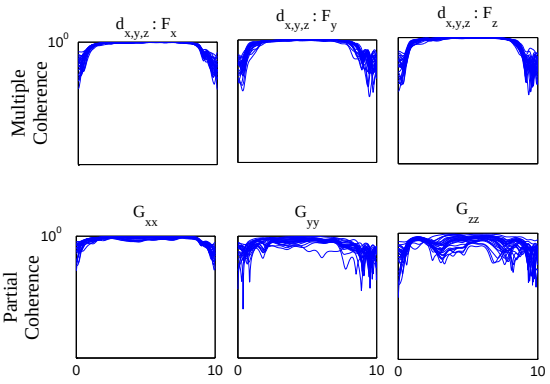

Fig. 4: Multiple and partial coherence values over the frequency range of [0 10] Hz. These indexes investigate the linear dependency of each output to all system inputs, and between single input and single output, respectively.

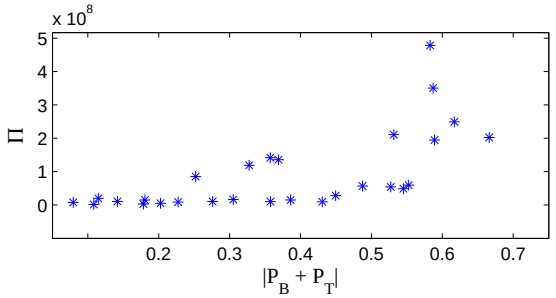

Fig. 5: Relationship between the summed muscular activities of the antagonistic pair ($|P_B + P_T|$) and the volume index (Π) of the experimentally identified endpoint stiffness matrices. A set of trials was randomly chosen from the overall number for this test.

Identification of $\overline{K_J}$ resulted in 14% average normalized error value over the calibration and test minimum activity trials, which is calculated by

$$e_{\overline{K_J}} = \sum_{i=1}^{n_{me}} \frac{\|K_c(\overline{K_J}, q_i) - K_{cei}\|}{\|K_{cei}\|}, \tag{12}$$

with K_c, K_{ce}, and n_{me} being the realized and the experimental Cartesian stiffness matrices and the total number of minimum activity trials, respectively.

Accordingly, identified $\overline{K_J}$ together with the computed co-contraction index $a_{cc}(P_B + P_T)$ were utilized to compute the modelling error for the overall number of high activation trials (n_{ha}) as follows

$$e_{a_{cc},\,\overline{K_J}} = \sum_{i=1}^{n_{ha}} \frac{\|K_c(a_{cc_i}, \overline{K_J}, q_i) - K_{cei}\|}{\|K_{cei}\|}, \tag{13}$$

which resulted in an average value of 23%. The relationship ($P < 0.0005$; $R^2 = 0.67$) between the summed muscular activities of the antagonistic pair ($|P_B + P_T|$) and the volume index

$$\Pi(K_{ce}) = \lambda_1.\lambda_2.\lambda_3$$

with λ_1, λ_2, and λ_3 being the eigenvalues of the experimentally identified endpoint stiffness matrix is illustrated in Fig. 5.

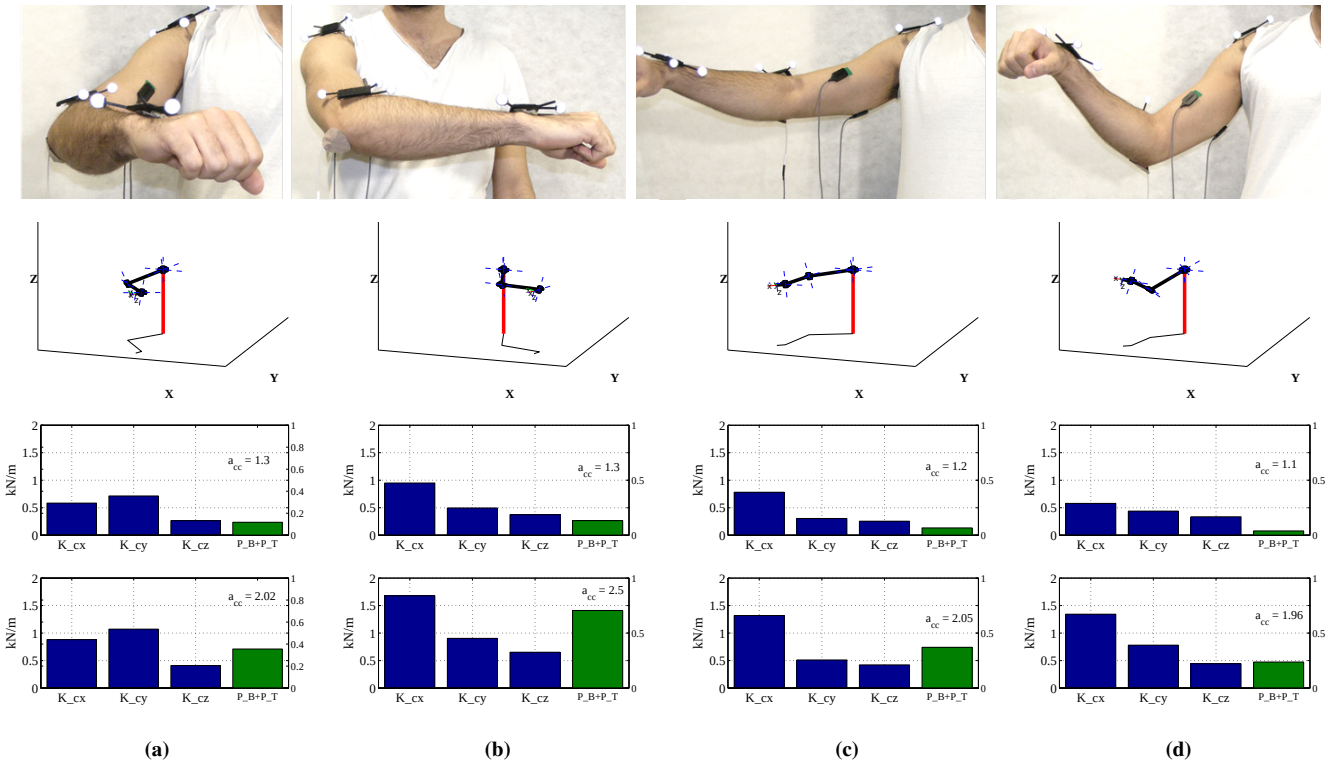

Fig. 6: Human arm configuration (upper plots), computed pose from the processing of the arm triangle (mid plots) and estimated Cartesian stiffness profiles along x (K_{cx}), y (K_{cy}), and z (K_{cz}) in different levels of the muscular activity ($P_B + P_T$) are illustrated. Proposed model provides the master with additional capabilities to realize the desired shape of the endpoint stiffness ellipsoid using arm configuration (e.g. compare lower two plots of (a) and (c) in which the most stiff direction varies between y and x directions), and its size (by taking into account the effect of cocontraction ($P_B + P_T$) in coordinated adjustments of the endpoint stiffness profile) for intuitive execution of a remote manipulation task.

B. Human Endpoint Stiffness Tracking

Figure 6 illustrates typical results of the tracking of the human arm endpoint stiffness profile in different arm geometry and muscular co-contraction levels. Arm configurations (upper plots) of the master were tracked using the arm triangle data and used for the estimation of the arm joint angles and the Jacobian. Estimated poses are illustrated in middle plots, using MATLAB's robotic toolbox. Computed arm Jacobian together with the co-activation index $a_{cc}(P_B + P_T)$ in two arbitrary contraction levels were used to calculate the Cartesian stiffness profiles along x (K_{cx}), y (K_{cy}), and z (K_{cz}) directions, in real-time (lower plots). Results suggest that chosen arm configurations have effectively modulated the direction of the realized endpoint stiffness profile, providing that its volume can be adjusted using muscular co-contractions.

The accompanying video [34] provides a simple example on the use of the proposed human arm endpoint stiffness estimation in a teleimpedance setup (see Fig. 7). In this video, the estimated stiffness profile and the tracked hand trajectories are realized by the Cartesian impedance controller of the KUKA robot in real-time. As demonstrated in the video, the subject is able to realize a desired direction and size of the Cartesian stiffness profile in the slave robot using his arm pose and the co-activation of the upper arm muscles, respectively.

A possible combination of the proposed model with the common-mode and configuration-dependent stiffness controller of the robot [35], will potentially achieve an effective and natural task execution in both master and remote sides.

VI. Conclusions

In this paper, a method for achieving effective interaction performance in a teleimpedance control setup was presented. To accomplish that, a novel, computationally efficient and real-time model of the human arm endpoint stiffness was proposed. Calibration and identification of the model parameters were carried out experimentally, using perturbation-based arm endpoint stiffness measurements in different arm configurations and co-contraction levels of the chosen muscles. Experiments evaluated the efficacy of the proposed model in generation of a desired stiffness profile, in real-time. Results suggest that the proposed model provided the master with the ability to regulate the direction of the major axes of the endpoint stiffness ellipsoid and its volume by choosing the arm pose and applying muscular co-contractions, respectively.

Future work will concentrate on the verification of the proposed model on more subjects and will include enhancements on the modelling of the joint stiffness matrix as an extension towards a larger workspace of the human arm.

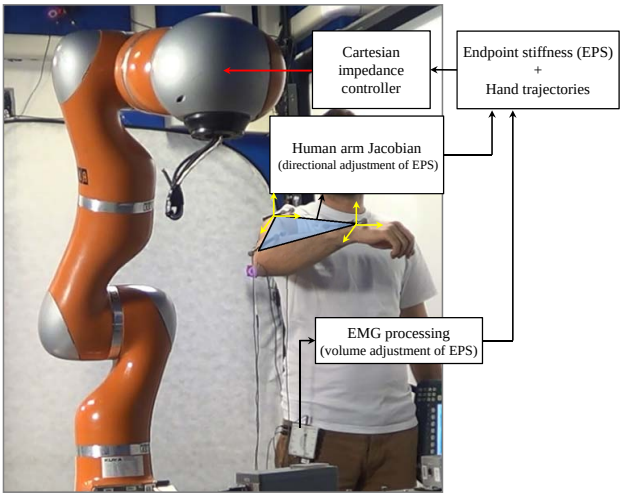

Fig. 7: Block diagram of the proposed teleimpedance controller. The arm Jacobian is computed by processing the arm triangle data and used for directional adjustment of the endpoint stiffness profile (EPS). Meanwhile, EMG signals are acquired from Biceps and Triceps Brachii, processed (700 Hz) and applied to account for the volume-adjusting component of the EPS. Resulting trajectories are then realized by a Cartesian impedance controller in 200 Hz.

REFERENCES

[1] B. Hannaford and R. Anderson, "Experimental and simulation studies of hard contact in force reflecting teleoperation," in *International Conference on Robotics and Automation*, 1988, pp. 584–589.

[2] G. Niemeyer and J. Slotine, "Telemanipulation with time delays," *International Journal of Robotics Research*, vol. 23, no. 9, pp. 873–890, 2004.

[3] A. Ajoudani, N. G. Tsagarakis, and A. Bicchi, "Tele-Impedance: Teleoperation with impedance regulation using a body-machine interface," *International Journal of Robotics Research*, vol. 31(13), pp. 1642–1655, 2012, http://www.youtube.com/watch?v=KPO6IO7Tr-Q.

[4] A. Ajoudani, N. Tsagarakis, and A. Bicchi, "Tele-Impedance: Preliminary results on measuring and replicating human arm impedance in tele operated robots," in *IEEE International Conference on Robotics and Biomimetics - ROBIO 2011*, 2011, pp. 216 – 223, youtube: http://www.youtube.com/watch?v=KPO6IO7Tr-Q.

[5] N. Karavas, A. Ajoudani, N. Tsagarakis, J. Saglia, A. Bicchi, and D. Caldwell, "Tele-impedance based assistive control for a compliant knee exoskeleton," *Robotics and Autonomous Systems*, 2014.

[6] A. Ajoudani, S. Godfrey, M. Bianchi, M. Catalano, G. Grioli, N. Tsagarakis, and A. Bicchi, "Exploring teleimpedance and tactile feedback for intuitive control of the Pisa/IIT softhand," *IEEE Transactions on Haptics*, vol. 7, pp. 203–2015, 2014.

[7] P. L. Gribble, L. I. Mullin, N. Cothros, and A. Mattar, "Role of cocontraction in arm movement accuracy," *Journal of neurophysiology*, vol. 89, no. 5, pp. 2396–2405, 2003.

[8] K. Akazawa, T. Milner, and R. Stein, "Modulation of reflex EMG and stiffness in response to stretch of human finger muscle," *Journal of Neurophisiology*, vol. 49, pp. 16–27, 1983.

[9] R. Trumbower, M. Krutky, B. Yang, and E. Perreault, "Use of self-selected postures to regulate multijoint stiffness during unconstrained tasks," *PLoS One*, vol. 4, no. 5, 2009.

[10] F. Mussa-Ivaldi, N. Hogan, and E. Bizzi, "Neural, mechanical, and geometric factors subserving arm posture in humans," *Journal of Neuroscience*, vol. 5, no. 10, pp. 2732–2743, 1985.

[11] E. Perreault, R. Kirsch, and P. Crago, "Voluntary control of static endpoint stiffness during force regulation tasks," *Journal of Neurophysiology*, vol. 87, pp. 2808–2816, 2002.

[12] D. W. Franklin, E. Burdet, R. Osu, M. Kawato, and T. E. Milner, "Functional significance of stiffness in adaptation of multijoint arm movements to stable and unstable dynamics," *Experimental brain research*, vol. 151, no. 2, pp. 145–157, 2003.

[13] D. Shin, J. Kim, and Y. Koike, "A myokinetic arm model for estimating joint torque and stiffness from emg signals during maintained posture," *Journal of neurophysiology*, vol. 101, no. 1, pp. 387–401, 2009.

[14] R. Osu and H. Gomi, "Multijoint muscle regulation mechanism examined by measured human arm stiffness and EMG signals," *Journal of Neurophysiology*, vol. 81, pp. 1458–1468, 1999.

[15] L. Selen, P. Beek, and J. V. Dieen, "Can co-activation reduce kinematic variability? a simulation study," *Biological Cybernetics*, vol. 93, pp. 373–381, 2005.

[16] D. G. Lloyd and T. F. Besier, "An emg-driven musculoskeletal model to estimate muscle forces and knee joint moments in vivo," *Journal of biomechanics*, vol. 36, no. 6, pp. 765–776, 2003.

[17] M. Kawato, "Internal models for motor control and trajectory planning," *Current opinion in neurobiology*, vol. 9, no. 6, pp. 718–727, 1999.

[18] M. Turvey, "Action and perception at the level of synergies," *Human Movement Science*, vol. 26, no. 4, pp. 657–697, 2007.

[19] T. Milner, "Contribution of geometry and joint stiffness to mechanical stability of the human arm," *Experimental Brain Research*, vol. 143, pp. 515–519, 2002.

[20] M. Ison and P. Artemiadis, "Proportional myoelectric control of robots: muscle synergy development drives performance enhancement, retainment, and generalization," *IEEE Trans. Robot*, 2014.

[21] C. Castellini, P. Artemiadis, M. Wininger, A. Ajoudani, M. Alimusaj, A. Bicchi, B. Caputo, W. Craelius, S. Dosen, K. Englehart *et al.*, "Proceedings of the first workshop on peripheral machine interfaces: going beyond traditional surface electromyography," *Frontiers in neurorobotics*, vol. 8, 2014.

[22] M. Ison and P. Artemiadis, "The role of muscle synergies in myoelectric control: trends and challenges for simultaneous multifunction control," *Journal of neural engineering*, vol. 11, no. 5, p. 051001, 2014.

[23] A. Ajoudani, N. Tsagarakis, and A. Bicchi, "On the role of robot configuration in cartesian stiffness control," in *International Conference of Robotics and Automation - ICRA*, 2015.

[24] S.-F. Chen and I. Kao, "Conservative congruence transformation for joint and cartesian stiffness matrices of robotic hands and fingers," *The International Journal of Robotics Research*, vol. 19, no. 9, pp. 835–847, 2000.

[25] P. Pigeon, L. Yahia, and A. G. Feldman, "Moment arms and lengths of human upper limb muscles as functions of joint angles," *Journal of biomechanics*, vol. 29, no. 10, pp. 1365–1370, 1996.

[26] G. Ettema, G. Styles, and V. Kippers, "The moment arms of 23 muscle segments of the upper limb with varying elbow and forearm positions: implications for motor control," *Human Movement Science*, vol. 17, no. 2, pp. 201–220, 1998.

[27] C. Fang and X. Ding, "A set of basic movement primitives for anthropomorphic arms," in *Mechatronics and Automation (ICMA), 2013 IEEE International Conference on*. IEEE, 2013, pp. 639–644.

[28] J. Denavit, "A kinematic notation for lower-pair mechanisms based on matrices." *Trans. of the ASME. Journal of Applied Mechanics*, vol. 22, pp. 215–221, 1955.

[29] X. Ding and C. Fang, "A novel method of motion planning for an anthropomorphic arm based on movement primitives," *Mechatronics, IEEE/ASME Transactions on*, vol. 18, no. 2, pp. 624–636, 2013.

[30] C. E. Clauser, J. T. McConville, and J. W. Young, "Weight, volume, and center of mass of segments of the human body," DTIC Document, Tech. Rep., 1969.

[31] S. L. Delp, F. C. Anderson, A. S. Arnold, P. Loan, A. Habib, C. T. John, E. Guendelman, and D. G. Thelen, "Opensim: open-source software to create and analyze dynamic simulations of movement," *Biomedical Engineering, IEEE Transactions on*, vol. 54, no. 11, pp. 1940–1950, 2007.

[32] G. Schreiber, A. Stemmer, and R. Bischoff, "The fast research interface for the kuka lightweight robot," in *IEEE Conference on Robotics and Automation (ICRA)*, 2010.

[33] C.-T. Chen and W.-D. Chang, "A feedforward neural network with function shape autotuning," *Neural networks*, vol. 9, no. 4, pp. 627–641, 1996.

[34] Video attachment, http://youtu.be/CVyNiud5K1s.

[35] A. Ajoudani, M. Gabiccini, N. G. Tsagarakis, A. Albu-Schäffer, and A. Bicchi, "TeleImpedance: Exploring the role of common-mode and configuration-dependant stiffness," in *IEEE International Conference on Humanoid Robots*, 2012.